energies

MDPI

Article

Hydrogen Enrichment Effect on Heat Flux from Plasma-Assisted Flames

Ignas Ambrazevičius, Rolandas Paulauskas, Justas Eimontas *, Nerijus Striūgas and Adolfas Jančauskas

Laboratory of Combustion Processes, Lithuanian Energy Institute, 44403 Kaunas, Lithuania; ignas.ambrazevicius@lei.lt (I.A.); rolandas.paulauskas@lei.lt (R.P.); nerijus.striugas@lei.lt (N.S.); adolfas.jancauskas@lei.lt (A.J.)

* Correspondence: justas.eimontas@lei.lt; Tel.: +37-037401976

Abstract

The European industries are transitioning from natural gas usage to renewable gases to enhance climate neutrality and energy security—therefore, hydrogen and ammonia gases could be great alternatives to natural gas. Hydrogen can be produced via electrolysis powered by renewable energy or from natural gas with carbon capture. Moreover, ammonia, composed of hydrogen and nitrogen, could also act as an energy carrier and storage medium. This study investigates the combustion process and efficiency of the hydrogen-enriched NH_3 and CH_4 blends using nonthermal plasma assistance. The experiments were performed with a gas burner with a thermal power of 1.30 kW using fully premixed gas blends. The nonthermal plasma was created with a high-voltage and high-frequency generator at 120 kHz and 8.33 kV. Time-resolved chemiluminescence data for OH* and NH_2* were captured using an ICCD camera, an MIR emission spectrometer and a thermal irradiance flux meter. The results indicated that nonthermal plasma enhances the flame stability and increases the infrared radiation intensity. The MIR spectroscopy showed an intensity increase of 13% for ammonia-hydrogen blends under plasma assistance and heat flux measurements showed a 15% increase for the 70% ammonia and 20% hydrogen mixture. These results demonstrate that plasma-assisted combustion can enhance the efficiency and stability of low-carbon fuel blends, facilitating their integration into current infrastructure while reducing greenhouse gas emissions.

Keywords: hydrogen; ammonia; plasma-assisted combustion; renewable gases; flame stability; combustion efficiency; infrared radiation; heat flux

Academic Editor: Albert Ratner

Received: 27 August 2025
Revised: 29 October 2025
Accepted: 4 November 2025
Published: 8 November 2025

Citation: Ambrazevičius, I.; Paulauskas, R.; Eimontas, J.; Striūgas, N.; Jančauskas, A. Hydrogen Enrichment Effect on Heat Flux from Plasma-Assisted Flames. *Energies* **2025**, *18*, 5880. https://doi.org/10.3390/en18225880

1. Introduction

The European gas market is undergoing a shift from natural gas to renewable gases, motivated by climate protection and energy security concerns [1]. Historically dependent on imports of natural gas, Europe is now exploring sustainable options such as hydrogen and ammonia. Hydrogen could be a zero-emission fuel if it is generated by renewable power using electrolysis (green hydrogen) or production from natural gas is coupled with carbon capture, storage and utilization (blue hydrogen) [2]. Moreover, blending hydrogen with natural gas could reduce overall emissions and reduce the new hydrogen infrastructure needs. Although H_2 blending is widely studied, there is still no robust scientific evidence on hydrogen enrichment limits in practical combustion applications showing how hydrogen enrichment could affect flame structure, dynamics, emissions and thermal irradiance. Prior reports suggest usable ranges of up to 42.2% vol for lean regimes and up to 20% vol for

rich flames. The evaluation of enrichment efficiency could be performed via high-speed OH* chemiluminescence and exhaust gas analysis, comparing pure CH_4 with different blends (the author suggested 31.2% and 42.2% H_2 at $\phi = 0.79 - 0.77$) and for rich blends (20% H_2 at $\phi = 1.16$) with plasma assistance [3]. Also, a hydrogen mixing with CH_4 could lower direct CO_2 emission and could improve stability at lean conditions by raising laminar flame speed [4]. In a recent study, modest H_2 fractions showed shortened reaction zones, a reduction in CO and unburned hydrocarbons via higher H*/O*/OH* radical concentrations [5]. Meanwhile, Bonuso et al. [6] have investigated how adding hydrogen to a low-swirl, non-premixed flame derived from an aero-engine air-blast atomizer changes flame structure and stability while holding the thermal output at 4.6 kW. The experiments have shown that hydrogen addition shortened the average flame length and widened the flame angle while shifting the brightest luminous emission toward the nozzle exit and reducing UV variance—evidencing an improved flame [6].

Another option is ammonia, which has significant potential for the European gas and industrial sectors as an alternative carbon-free energy carrier [7]. It can be produced from green hydrogen and nitrogen, stored at moderate conditions (−33 °C at 1 bar or 0.8–1.0 MPa at room temperature) [8]. Liquid ammonia contains 106 kg H_2 per cubic meter and liquid hydrogen 70 kg H_2 per cubic meter while storage costs are 26–30 times lower than hydrogen [9]. Multiple pilot programs across Europe are assessing the integration of ammonia into energy infrastructure. This could enable seasonal energy storage, reduce CO_2 emissions process in sectors that are difficult to decarbonize and enhance the reliability of renewable energy supply. As a result, ammonia–methane blends could be used as the transitional solution or alternative solutions to pure hydrogen installations. However, the specific blending ratios must be carefully managed to mitigate the technical combustion challenges [10]. These challenges include high ignition energy, slow flame speed (~7 cm/s vs. methane's ~35 cm/s), poor stability, low efficiency and elevated NO_2, NO emissions and NH_3 slip due to poor combustion conditions [11]. Co-firing with hydrogen or hydrocarbons can improve flame stability [12]. Methane–ammonia blends show wider flammability limits and NO_x emission reductions [13]. Industrial utilization of ammonia itself could reach up to 30% NH_3 in kilns and furnaces where the direct flames are used [14].

Although hydrogen and ammonia holds potential to replace natural gas, several technical issues need to be overcome. One of the major problems is the reduced radiant heat release during the combustion process. Hydrogen and ammonia flames usually provide low emissivity when compared to methane or other hydrocarbon fuels due to mitigation of soot formation [15]. Hwang and Gore [16] determined that low soot production leads to reduced radiative heat transfer from the flame. This will impact on the performance of methane-designed gas burners and may necessitate redesigning or changing them to enable efficient combustion and heat transfer processes. Moreover, hydrogen has a faster flame speed than methane could lead to backflash and cause more wear and tear on burner components resulting in need to modify burner design to enable a secure and stable combustion process. On the other hand, ammonia combustion can produce NO and NO_2 emissions that require effective mitigation strategies such as selective catalytic reduction (SCR) systems to comply with environmental standards [17].

These technical problems could be resolved with plasma-assisted combustion technology. This technology enhances the combustion process by generating reactive species that improve flame stability and increase flammability limits [18]. Unlike thermal plasma, nonthermal plasma operates at low gas temperature but with high electron energy (1–10 eV)—enabling continuous generation of reactive radicals (OH*, NO*, NH_2*) [19]. These radicals could accelerate combustion reactions while minimizing energy losses. Plasma-assisted combustion demonstrated the reduction in ignition delay, extended lean

blowout limits and stabilized premixed and swirl flames [20]. Nonthermal plasma enhances NH_3 and H_2 blends' combustion by supplying radicals (H*, O*, OH*, NH_x*) that accelerate NH_3 cracking to H_2 and N_2, shorten ignition delay and raise burning velocity [21]. Irace PH et al. [22] using a nanosecond repetitively pulsed nonthermal plasma reformer demonstrated dramatic ignition enhancement for ammonia/air mixtures. H_2 yield from 0.03 to 0.2% from NH_3 reforming was determined at 200 kHz and 1500 pulses [22]. Another work [23] focused on ammonia/air premixed flame stabilization by coupling swirling flow and plasma discharges and determined that plasma assistance reduces the lean blowout limit. Similar findings were provided by Sun et al. [24]. Authors determined the effect of plasma discharge timing and observed that lean blow-out limits are reduced by increasing energy density per pulsed discharges. Positive results on ammonia flame stability due to plasma discharge influence have been presented by Choe et al. [25]. Also, few recent papers present thermal effects due to plasma assistance. For example, Wang et al. [26] performed numerical modeling of ammonia combustion using gliding arc plasma and determined that during plasma discharges the gases are heated by 200 K. Other work [27] also observed thermal effect from nonthermal plasma discharge in ammonia/hydrogen flames but authors noted that both thermal and chemical effect from plasma discharges enhances the burning velocity of the flame. Also, studies related to plasma-assisted combustion [28–30] indicates that during discharges the ozone is generated, which leads to more intensive fuel oxidation, increased flame temperature and could intensify soot formation [31].

However, there still exists a gap considering thermal characteristics of alternative fuel flames, especially assisted by nonthermal plasma, which could ensure flexibility of fuel use [32]. This work is investigating thermal and spectral flame characteristics, such as chemiluminescence and infrared radiance, across ϕ = 0.81, 0.71, 0.62 fuel-to-air ratios for CH_4, CH_4–H_2 and CH_4–NH_3 and H_2–NH_3 blends.

2. Materials and Methods

Experiments were performed using a premixed gas burner with a thermal power output of 1.30 kW. The nonthermal gliding arc plasma was formed inside the burner to perform plasma-assisted combustion of CH_4, H_2 and NH_3 blends and various techniques were used for flame diagnostics. More details are provided in the sections below.

2.1. Plasma-Assisted Combustion Rig

Figure 1 presents the experimental combustion rig. The plasma-assisted burner consists of a conical electrode with a 20 mm outer diameter at its widest point, made from stainless steel and connected to a high-voltage generator acting as anode. The ground electrode (cathode) consisted of a cylindrical stainless-steel body with an internal diameter of 22 mm, therefore the gap between anode and cathode were 1 mm. The exact gap dimensions were selected experimentally considering the combustible gas properties, flows and the operation voltage along the gap between the anode and cathode [33]. The upper section of the burner was fitted with a quartz glass tube to facilitate flame stabilization and visual observation. More details on the burner are presented in [34].

The combustion air was supplied by the compressor via silica gel drying system (to remove residue moisture) at 1.5 bar pressure. Ammonia (NH_3), methane (CH_4) and hydrogen (H_2) gases were supplied from gas cylinders and flows were controlled using mass flow controllers (Brooks SLA5860, Brooks Instrument, Hatfield, PA, USA). In total, four mass flow controllers were used: three for combustible gases and one for compressed air. All mass flow controllers were factory-calibrated individually and specifically for air, methane, ammonia and hydrogen and additionally validated using the mass flow instrument Alicat PCU-portable mass flow calibration kit (Alicat Scientific, Tucson, AZ,

USA). These controllers maintained the flow according to set values, ensuring consistent combustion performance by keeping constant the fuel-to-air equivalence ratio.

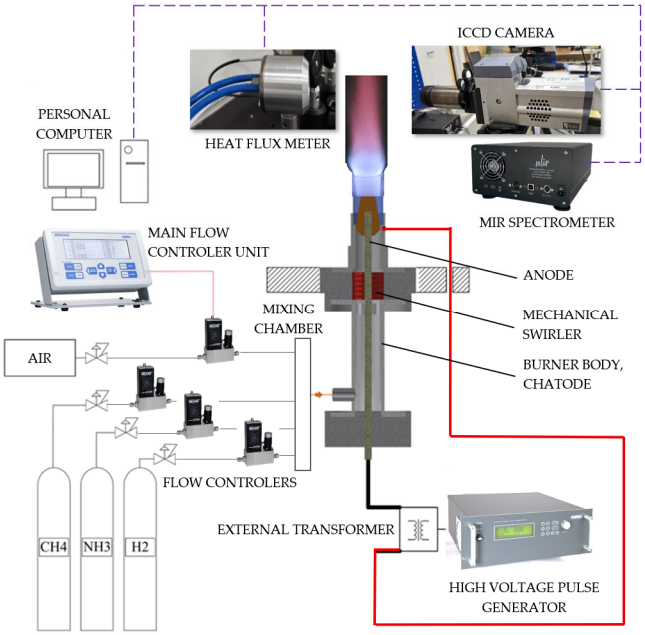

Figure 1. Plasma-assisted combustion rig.

The mixture was prepared by supplying combustible gases (CH_4, NH_3, H_2) and compressed air via tubes to the mixing chamber, then the mixture was directed to the burner. Also, the gas burner was equipped with the static mechanical swirler with vanes that create a 40° angle exit. This mechanical swirler created a swirling motion of mixture inside the burner body [35]. The swirling flow was directed through the burner to the narrowest point between the anode and cathode; here, nonthermal plasma in the form of a gliding arc was created and due to the swirling motion of mixture, the discharge arcs started to rotate around the anode covering all cross sections of the gas burner outlet [36].

A high-voltage plasma generator G2000 (Redline TechnologiesElektronik GmbH, Baesweiler, Germany), with a maximum voltage of 8.33 kV and a frequency range of 0–500 kHz, was used to create the plasma discharge. Experiments were conducted using a 200 V (6.6 kV after the transformer) voltage and a frequency of 120 kHz. These nonthermal plasma parameters were based on previous experiments, indicating that these values are optimal for combustion improvement with nonthermal gliding arc plasma [37]. In addition, before starting the experiments, it was determined that the aerodynamic properties of the fixed mechanical swirler leads to different flow velocities caused by different gas compositions and the swirling motion affects both the flame stability and nonthermal gliding arc plasma behavior negatively if the overall mixture flow is not sufficient. At low gas flow rates, the gliding arc was unstable, forming elongated, non-rotating arcs that interfered with the generation of active species and compromised flame stability. To mitigate this instability the permanent neodymium ring magnets were installed. The used magnet type was an N42 Nd–Fe–B ring magnet (OD 40.0 ± 0.1 mm, ID 22.0 ± 0.1 mm, height 10.0 ± 0.1 mm), axially magnetized through the 10 mm thickness. The specified holding force was 28 kg (~275 N)—two magnets in total were used. Such an upgrade ensured stable plasma discharges in the flames.

2.2. Luminous and Non-Luminous Emission Spectroscopy and Thermal Irradiance Analysis

The combustion process was investigated by an optical diagnostic system developed to study the spatial variation in excited species OH* (310 ± 10 nm) and NH_2* (632 ± 10 nm) at

atmospheric pressure. Images of flame chemiluminescence were captured by an ICCD camera (Andor iStar DH734, Andor Technology Ltd., Belfast, Northern Ireland, UK) using hard-coated bandpass filters as mentioned above and final images were produced by averaging 30 sequential exposures with 0.04 s of each exposure. Non-luminous flame emissions were measured by mid-infrared (MIR) spectroscopy using an NLIR S2050–400 spectrometer (NLIR ApS, Farum, Denmark) operating over 2000–5000 nm wave lengths. This instrument (NLIR 2.9.0) acquired each spectrum as an average of 30 scans per 100 milliseconds with the 130 mm axial distance from the flame [38].

For the thermal irradiance measurement, the water-cooled thermopile SBG01 heat flux sensor (Hukseflux Thermal Sensors B.V., Farum, Denmark) [39] was positioned at the same axial distance as the NLIR spectrometer (NLIR ApS, Farum, Denmark). This Gardon and Schmidt–Boelter-type sensor, equipped with a black absorber, measured heat flux up to 50 kW/m^2. No additional optical filter was used to filter different irradiance wavelengths for heat flux measurement instrument. The sensor generated an output voltage proportional to the incoming thermal irradiance, which was recorded using a Rigol DM 3068 digital multimeter (RIGOL Technologies, Inc., Beijing, China) connected to a personal computer [40]. The final value of the heat flux intensity for each gas blend and air/fuel ratio was derived as the average of 10 scans.

2.3. Flame Temperature Measurement

Flame temperature was measured at three locations within the flame core. Each measurement point was predefined, and the thermocouple was positioned at the same location for every run. At each point, the acquisition window was 3 s, and the maximum temperature observed during that interval was recorded. A type R (Pt–Pt13%Rh) thermocouple with a 0.2 mm external diameter, rated to 1700 °C, was used. Cold-junction compensation was provided by a K-type thermocouple immersed in an ice-water bath. Signals from both thermocouples were acquired and processed with a Pico TC-08 thermocouple data logger (Pico Technology Limited, St Neots, Cambs, UK). The setup was validated using an ice bath (0 °C), boiling water at atmospheric pressure (100 °C), and a preheated, calibrated oven set to 800 °C. In similar applications the true flame temperature was within ≈1.1% accuracy (≈17 K at ~2000 K) in H_2/air flames using double S-type thermocouples, the notable uncertainties were observed due to the thermocouple junction diameter [41]. Furthermore, radiative losses could influence in 200 K bias from true flame temperature yields ≈ ±70 K uncertainty for a 0.20 mm probe over 1100–1800 K [42]. To correct the thermocouple readings, the temperature-compensation method of Cafiero et al., developed for $H_2/CH_4/CO$ flames across air-to-fuel ratios of ϕ = 0.8, 1.0, 1.2 and an applied 227–1427 °C temperature range was also used [43]. The mathematical correction factors eliminating the heat loss from the thermocouple tip, the outcomes of R type thermocouple validation experiments and thermocouple manufacturer-supplied correction factors for the Type R thermocouple were used to adjust the flame temperature measuring readings.

2.4. Methodology for Conducting Combustion Experiments

The experiments were conducted using various hydrogen-enriched ammonia and methane blends at different fuel-to-air ratios. The detailed composition of these mixtures is provided in Table 1. Gas blends and flow rates were calculated to maintain a constant thermal combustion power of 1.30 kW. Detailed stoichiometric calculations were prepared in accordance with the standard EN12953:11:2003 [44]. The calculations determined the required combustion air flow, gas flow rates, adiabatic flame temperatures and calorific values of blends.

Table 1. Gas hydrogen-enriched ammonia and methane blends combustion calculation results.

Parameter	Units	100%CH_4	80%CH_4 + 20%NH_3	80%CH_4 + 20%H_2	10%CH_4 + 70%NH_3 + 20%H_2
Fuel-to-air ratio	-	0.81–0.62	0.81–0.62	0.81–0.62	0.81–0.62
Adiabatic flame temperature	°C	1748	1732	1762	1670
Gas calorific value	kJ/Nm^3	35,833	31,578	30,863	15,797
Combustion power of the burner	kW	1.30	1.30	1.30	1.30

The equilibrium flue-gas compositions and adiabatic flame temperatures were calculated for hydrogen-enriched ammonia and methane blends over a range of mixing ratios. The experiments included CH_4–NH_3, CH_4–H_2 blends and H_2–NH_3 with a 10 vol% CH_4 blend to maintain flame stability. The hydrogen content was varied up to 20–30 vol% for these blends. Table 1 shows that the highest adiabatic temperatures were calculated for a mixture of 80% methane and 20% hydrogen, while the lowest were calculated with a mixture of 70% ammonia and 20% hydrogen.

3. Results

The objective of these plasma-assisted combustion experiments is to investigate the thermal irradiation of flames produced by various gas blends, the distribution of excited hydroxyl (OH*) and amidogen (NH_2*) species, infrared spectral characteristics, flame temperature and to analyze heat flux. Nonthermal plasma-assisted combustion could increase the infrared spectrum intensities by increasing the emission of infrared radiation due to the formation of carbon dioxide (CO_2) and water vapor (H_2O), both of which exhibit strong infrared absorption and emission bands. Moreover, the production of intermediate species such as OH* and NH_2* should increase the net radiative heat release [45,46].

3.1. Radiative Flame Characteristics

Major combustion products such as carbon dioxide (CO_2) and water vapor (H_2O) exhibit strong infrared absorption and emission due to their vibrational and rotational transitions [19,47]. In reference it is noted that CO_2 emits at wavelengths around 2000 nm and 4400 nm; H_2O emits between 1800 and 2000 nm and coincides with CO_2 emissions at approximately 2800 nm [47,48]. Recent studies also indicate that a peak intensity at 2500 nm is attributed to H_2O. Additionally, Henrion et al. found that the highest intensities are at wavelengths of 4300–4500 nm due to CO_2 emissions [49].

Figure 2 shows the infrared spectra analysis during the combustion of gas blends without plasma assistance, highlighting CO_2 and H_2O as the primary thermal emitters at different wavelengths. Infrared analysis of the H_2O and CO_2 bands have showed clear mixture-dependent changes in intensity: the 80% CH_4 and 20% H_2 blend produced the strongest H_2O and combined H_2O + CO_2 band intensities. In contrast the blend of 70% NH_3 and 20% H_2 yielded lower infrared intensities and for CO_2 only bands, the weakest response occurred with 70% NH_3 and 30% H_2 blend. These results demonstrate that CO_2 significantly influence the flue-gas radiative properties. Potentially adding a small amount of CO_2 to hydrogen (H_2)-enriched gas blends can initially increase total emissivity [48].

In comparison, Figure 3 represents the same hydrogen-enriched NH_3 and CH_4 blends with the nonthermal plasma assistance at fuel-to-air ratio ϕ = 0.81: the mid-infrared intensities strengthened across all monitored bands. For the 80% CH_4 and 20% H_2 blend, both the isolated H_2O wave bands and the overlapped H_2O + CO_2 region (near ~2700 nm) increased significantly. The 70% NH_3 and 20% H_2 blend showed a weaker intensity increment and was notable only in H_2O corresponding wavelength region, whereas CO_2-only bands

remained comparatively weak as it was limited by the fuel chemistry. These findings are consistent with established plasma-assisted combustion mechanisms in which nonthermal plasma generates H*/O*/OH* (and, for NH_3 fuels, NH_2) radicals and vibrationally excited molecules, accelerating oxidation chemistry [19].

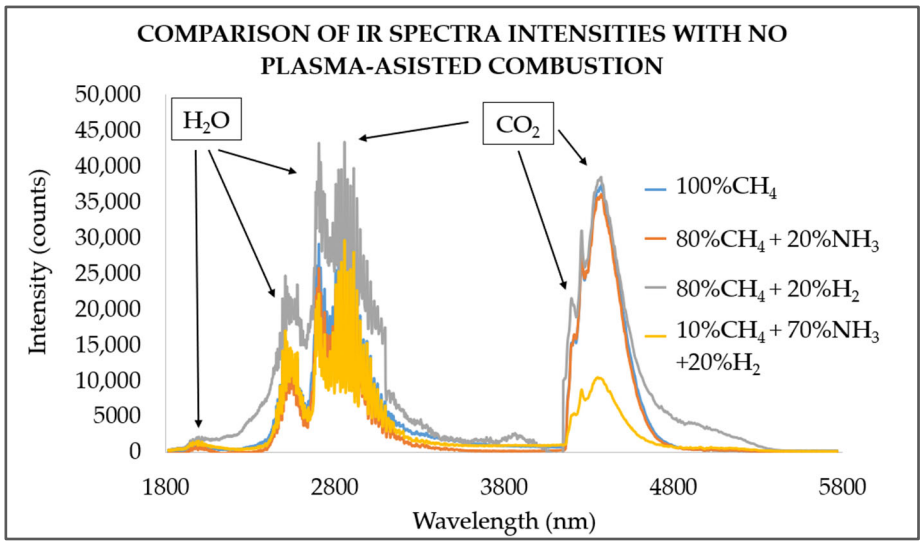

Figure 2. Infrared radiation spectra intensities for different hydrogen-enriched NH_3 and CH_4 blends with no plasma assistance at 0 kHz at ϕ = 0.81.

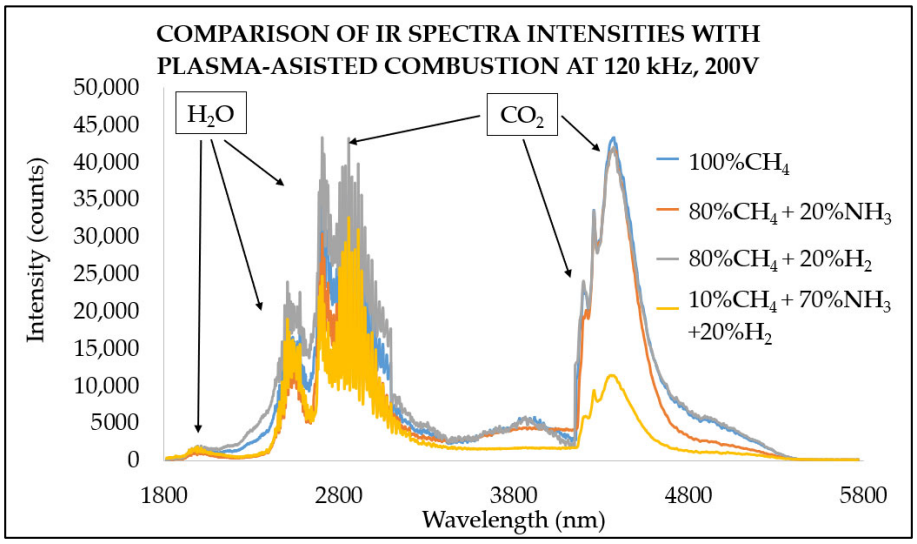

Figure 3. Infrared radiation spectra for different hydrogen-enriched NH_3 and CH_4 blends with plasma assistance at 120 kHz and 8.33 kV at ϕ = 0.81.

In Figure 4, a comparison of IR spectrum intensities for 70% ammonia and 20% hydrogen blends with and without plasma assistance are shown in one graph. The low-carbon content with only 10% methane in the gas blend resulted in the highest intensities in the H_2O and mixed H_2O + CO_2 bands and the lowest in the CO_2-only bands. When nonthermal plasma was applied, the general spectrum intensity increased by 13%. A similar phenomenon was noted for the CO_2 band alone, indicating that for carbon-free gas mixtures, additional CO_2 could enhance spectral intensities. However, more detailed experimental studies on the effects of additional CO_2 injection are needed to evaluate the underlying mechanisms in low-hydrocarbon content gas blends.

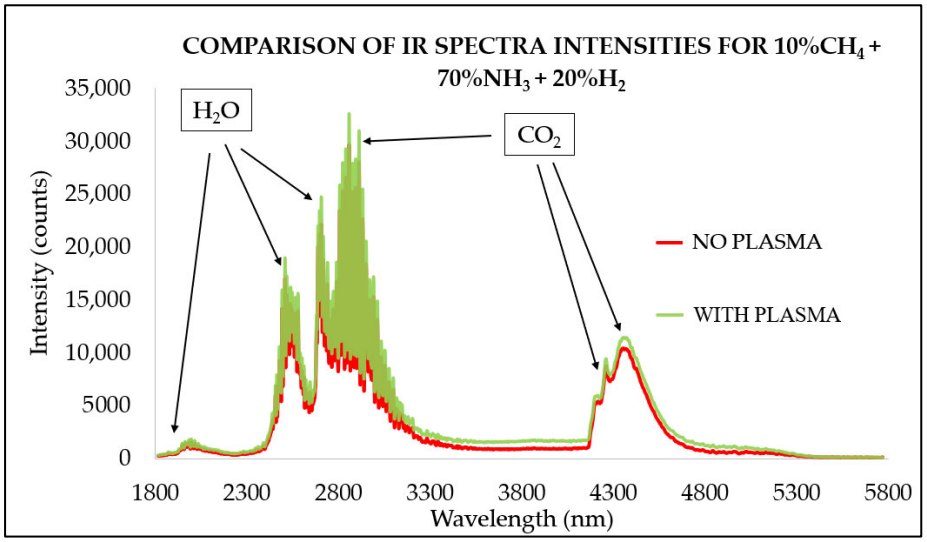

Figure 4. Infrared radiation spectra for 70% NH_3 and 20% H_2 mixture with plasma at 120 kHz and 8.33 kV and no plasma assistance at ϕ = 0.81.

For the understanding of nonthermal plasma influence on flame characteristics, spatial chemiluminescence emissions of OH* and NH_2* were captured with an intensified camera (ICCD) and the data were processed to produce flame images on a common intensity scale for both species. An NH_2* bandpass filter was used for mixtures containing ammonia, and an OH* bandpass filter was applied to all mixtures.

Figure 5 shows ICCD images of 100% methane using the OH* and NH_2* bandpass filters with plasma assistance at 120 kHz and 8.33 kV at fuel-to-air ratio of ϕ = 0.81. The ICCD images of the 100% methane flames served as the primary reference to assessing how nonthermal plasma assistance affects flame behavior and thermal irradiance. These images were compared with hydrogen-enriched methane (CH_4–H_2) and ammonia–hydrogen (NH_3–H_2) blends. Under nonthermal plasma assistance, OH* chemiluminescence intensified near the anode and indicated enhanced local OH* production. Under nonthermal plasma assistance, high-energy electrons in a non-equilibrium energy distribution dissociate methane via electron impact. Generating CH_X fragments together with H and H_2, the electron impact also affects O_2 ($e + O_2 \rightarrow 2O + e$). These two mechanisms generate OH radical increment, while vibrational excitation and ion–molecule pathways further promote reforming toward H_2 and CO/CO_2. These mechanisms are consistent with the observed intensification of OH* chemiluminescence near the anode and with the upstream shift in the luminosity peak under plasma-on conditions.

The similar results were obtained with the NH_2* filter showing increased spatial emission with the nonthermal plasma assistance. For the 100% methane case, NH_2* production was lower due to the absence of ammonia; the observed increase in NH_2* signal is attributed to nitrogen chemistry originating from the combustion air under plasma activation. The nonthermal plasma improved flame stability and shifted the flame core downstream for 100% methane at a fuel-to-air ratio of ϕ = 0.81.

Figure 6 shows a mixture with 80% methane and 20% hydrogen using the OH* and NH_2* bandpass filters. Hydrogen enrichment strongly modified chemiluminescence in methane flames; our experiments showed the increase in OH* signal intensity. In reference [50] to where similar experiments were conducted at higher hydrogen fractions or rich conditions, OH*/CH* becomes non-monotonic. Thus, hydrogen enrichment complicates chemiluminescence-based monitoring, linking radical pathways to both combustion regime and flame structure. Using the NH_2* filter with plasma assistance showed enhanced flame stability, with increased spatial emissions observed in nonthermal plasma operation

regime. During the plasma assistance, the flame core was shifted up for the mentioned gas mixture at a fuel-to-air ratio ϕ = 0.81. These results indicate a positive thermal and kinetic effect of plasma, expanding the flame-covered zone and intensifying OH*. In this case, production of NH_2* radicals was lower due to ammonia absence in the 80% methane and 20% hydrogen blend and observed NH_2* radical intensity increment was caused by nitrogen gas that was in combustion air. Moreover, the methane blends with 20% hydrogen displayed bright red flames with distinct methane and hydrogen combustion zones.

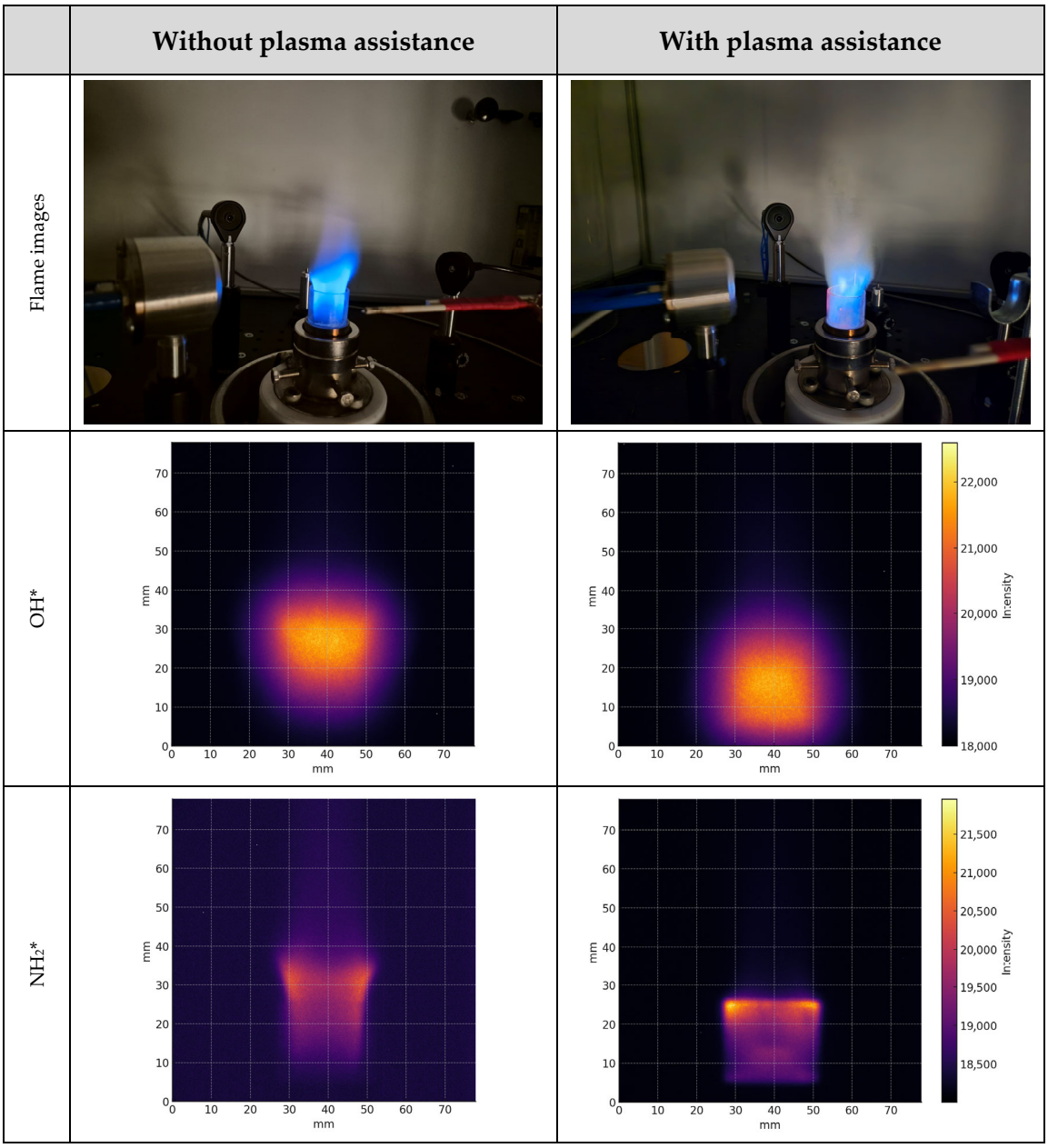

Figure 5. Flame images and spatial distribution of OH* and NH_2* from methane flame under plasma assistance at 120 kHz and 8.33 kV and without plasma assistance at ϕ = 0.81.

Additionally, Figure 7 illustrates 70% ammonia and 20% hydrogen blends using the NH_2* and OH* bandpass filters with and without plasma assistance. Plasma-assisted combustion has widened the flame and enhanced flame stability leading to increased spatial emissions observed at higher frequencies. It was also observed that the flame core was significantly lower compared to combustion without plasma. On average, with plasma assistance, the flame core was 20 mm lower for 70% ammonia (NH_3) and 20%

hydrogen (H_2) blends and at fuel-to-air ratio ϕ = 0.81. These results indicate a positive thermal and kinetic effect of plasma, expanding the flame-covered zone and intensifying OH* and NH_2* emissions. Moreover, nonthermal plasma creates a high concentration of short-lived radicals (H, O, OH, N, NH, NH_2) and vibrationally excited species before significant thermal heating occurs. These species accelerate the initiating chain-branching reactions, thereby shortening the local ignition delay.

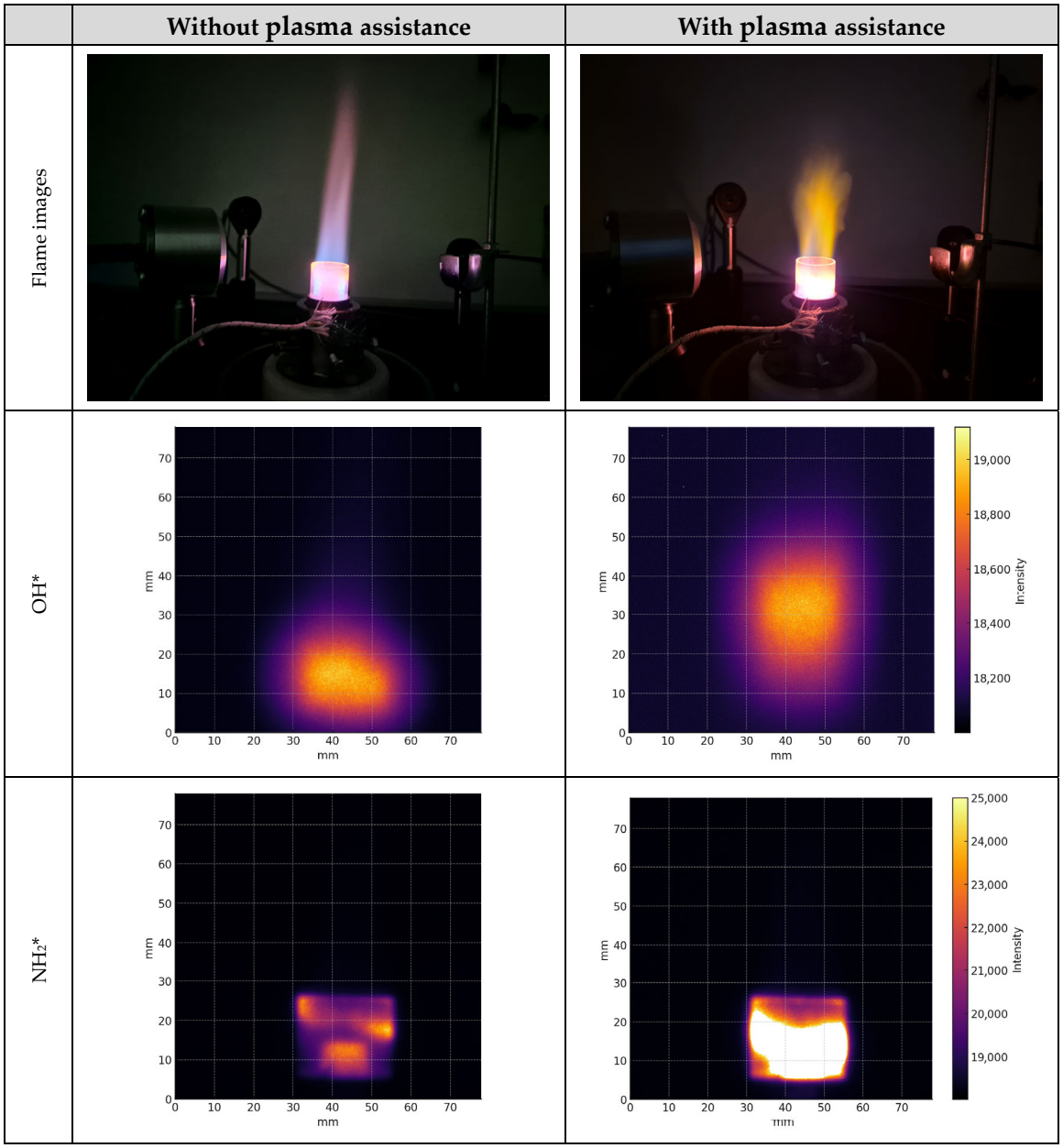

Figure 6. Flame images and spatial emissions of OH* and NH_2* from 80% methane and 20% hydrogen mixture flame under plasma assistance at 120 kHz and 8.33 kV and without plasma assistance at ϕ = 0.81.

The injection of hydrogen into gas mixtures significantly impacted flame characteristics and stabilized the flame, especially in fuel-lean conditions, due to its high diffusivity and reactivity. With nonthermal plasma assistance, the flame exhibited increased intensity and enhanced stability. In the case of blends comprising 70% ammonia and 20% hydrogen at a fuel-to-air ratio ϕ = 0.62, the flame became unstable and tended to extinguish under

extremely lean conditions. However, with the introduction of plasma assistance, this mixture combusted efficiently without any issues.

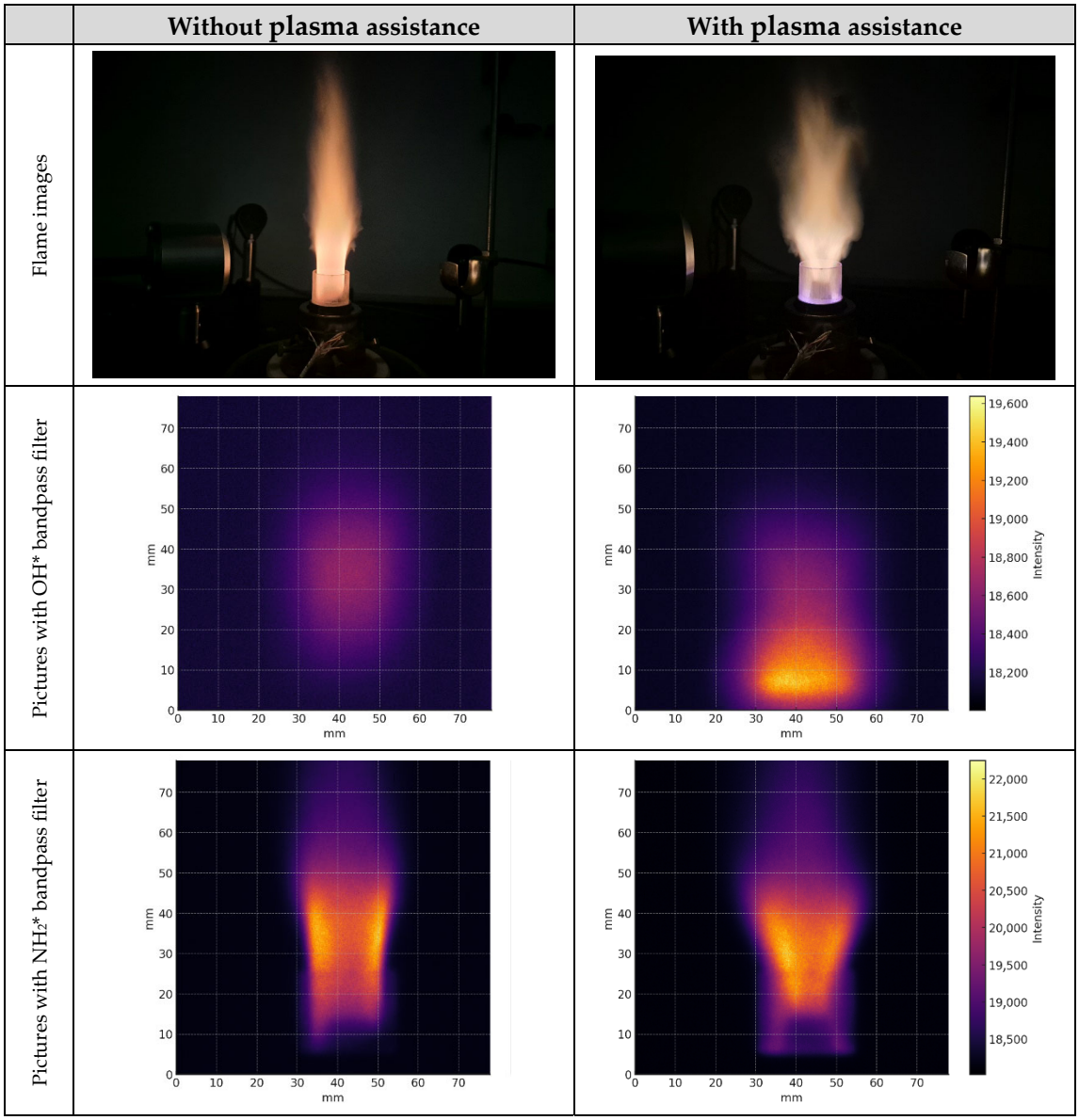

Figure 7. Flame images and spatial emissions of OH* and NH2* from 70% ammonia and 20% hydrogen mixture flame under plasma assistance at 120 kHz and 8.33 kV and without plasma assistance at $\phi = 0.81$.

3.2. Flame Characteristics

To determine the plasma effect on thermal flame characteristics, the heat flux of the flames was measured at $\phi = 0.81, 0.71, 0.62$ fuel-to-air ratios for hydrogen-enriched methane and ammonia gas blends. Figure 8 presents the heat flux distribution emitted from flames, showing that the highest flux that occurred was observed for the 80% methane–20% hydrogen blend, whereas the lowest was observed for the 70% ammonia 20% hydrogen blend. Green bars (NP) denote operation without plasma and blue bars (P) with nonthermal plasma. The red and purple curves overlay the calculated H_2O and CO_2 volume fractions, respectively. Samples on the x-axis are ordered by increasing calculated adiabatic flame temperature. Together with the heat flux, flame temperature measurements are represented in this graph too. The yellow line (temperature with plasma) lies above the light-blue line (without plasma) across the dataset, and the gap widens at $\phi = 0.62$ group.

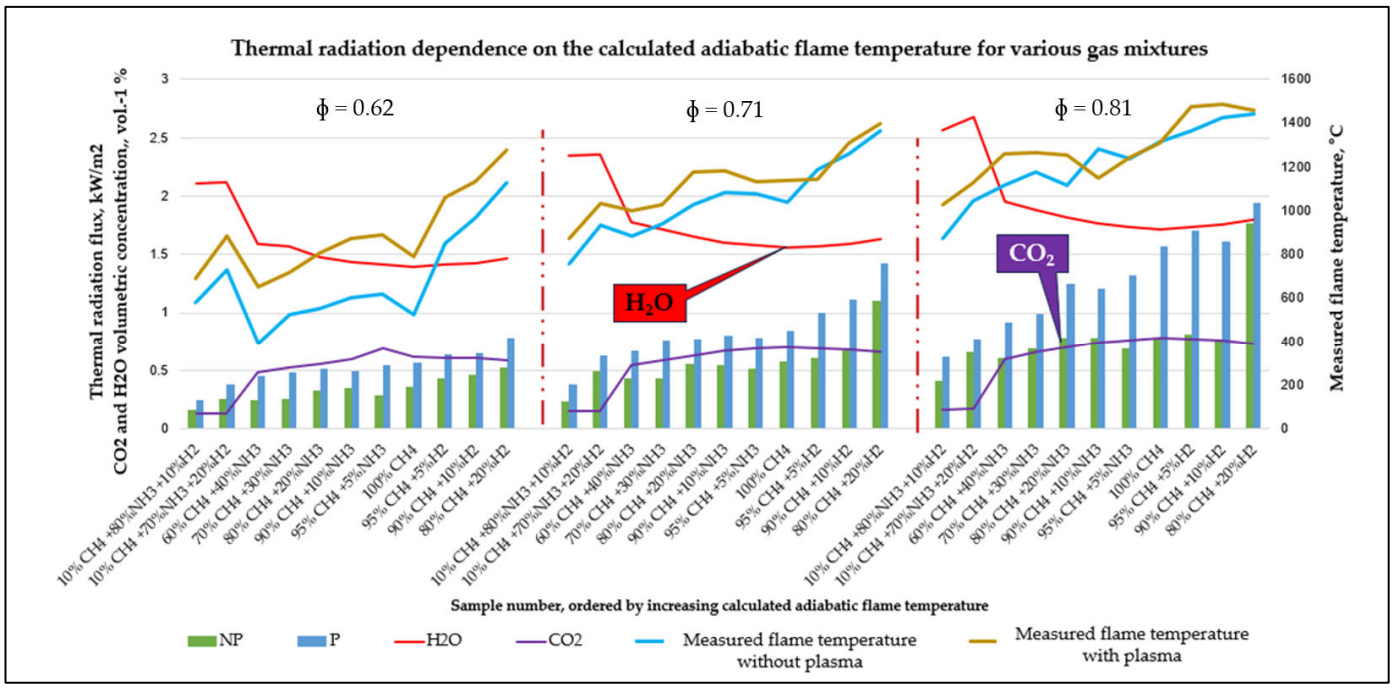

Figure 8. Flame heat flux measurements for hydrogen-enriched methane and ammonia blends at ϕ = 0.81, 0.71, 0.62 fuel-to-air ratios.

The nonthermal plasma combustion assistance increased the heat flux values, with the highest increase observed for 100% methane and progressively lower increments for methane–ammonia and ammonia–hydrogen blends. This graph represents heat flux and flame temperature measurements with and without nonthermal plasma assistance for various fuel-to-air ratios at ϕ = 0.81, 0.71, 0.62. Furthermore, for the low-carbon blend of 70% ammonia and 20% hydrogen, the increase in heat flux intensity was 15%. This is a significant increment for mixtures with low-carbon content, highlighting the efficacy of plasma assistance in enhancing combustion properties even in low-carbon scenarios.

The triatomic species fractions (H_2O, CO_2) vary with different compositions of CH_4, CH_4–H_2 and CH_4–NH_3 blends, whereas H_2–NH_3 blends exhibit a higher H_2O fraction as shown in Figure 8. The strong co-variation between heat flux and H_2O together with CO_2 was observed indicate that H_2O and CO_2 play crucial roles in radiative heat release and flame thermal irradiance.

The infrared spectral analysis confirms the trends shown in Figure 8—nonthermal plasma-assisted combustion increases the integrated intensity of H_2O bands near 2700 nm across all equivalence ratios, while CO_2 features (4300 nm band) exhibit smaller composition-dependent changes—particularly in NH_3–H_2 mixtures, where CO_2 is low. As a result, the heat flux measurement results and the infrared spectra show strong correlation between each other. Under nonthermal plasma assistance, flame temperature increases only slightly at fuel-to-air ratios ϕ = 0.62; however, the infrared spectral intensity rises significantly—most predominantly in H_2O bands and in mixed H_2O + CO_2 regions. Consequently, the observed increase in radiative heat flux is driven primarily by enhanced H_2O and CO_2 emissions. The nonthermal plasma generates a non-equilibrium electron population that promotes electron-impact dissociation and excitation (e.g., of $CH_4/O_2/H_2O$), elevating the local concentrations of H, O and OH and accelerating chain-branching reactions. These kinetics modestly raise flame temperature while increasing the population of radiating species and the effective radiative path length, thereby amplifying H_2O-dominated emission and the overall spectral intensity, even in NH_3-rich (low-carbon) blends where CO_2 is intrinsically limited.

4. Discussion

The combustion experiments of the hydrogen-enriched ammonia and methane blends were conducted to examine the thermal radiation and flame characteristics under plasma-assisted combustion. These experiments revealed that the elevated flame temperatures caused by plasma assistance increased infrared emission in accordance with the Stefan–Boltzmann law, which relates radiative heat flux to the fourth power of temperature. In addition, nonthermal plasma facilitated the formation of intermediate species such as OH*, CH* and other radicals. These species affect the combustion process by stabilizing the flame and raising its temperature, thereby indirectly enhancing infrared radiation.

During the experiments, methane–hydrogen mixtures produced intense red flames, where the presence of hydrogen increased both the flame temperature and the burning velocity. In contrast, the 70% ammonia–20% hydrogen blend formed the longest flame, displaying a flow pattern that closely resembled laminar combustion.

Nonthermal plasma significantly improved flame stability and thermal radiation intensity. Plasma-assisted flames were more turbulent and stable with distinct V-shape form and elevated flame cores that could be observed in ICCD images with transmission bands of OH*, while the NH_2* filter resolved a notable result only on gas blends containing NH_3. With nonthermal plasma assistance, flame temperatures increased slightly. For the 100% methane flame, the temperature rose from 1307 °C to 1316 °C, while for other gas mixtures the increase was about 100 K.

Moreover, nonthermal plasma increased infrared intensities' counts across all tested gas blends. In the 80% methane and 20% hydrogen blends, significant enhancements were observed in the H_2O and CO_2 spectral bands. The 70% ammonia and 20% hydrogen mixture, which initially exhibited weak infrared intensities counts, also showed a marked increase. The 80% methane and 20% hydrogen mixture exhibited the highest infrared (IR) emission counts for both H_2O and combined H_2O plus CO_2 spectra.

The use on nonthermal plasma during the gas blends' combustion also increased heat flux by approximately 15% in the low-carbon 70% ammonia and 20% hydrogen mixture. Plasma-assisted combustion elevated flame temperatures and promoted the formation of intermediate chemical species. These changes improved combustion efficiency, increased IR radiation intensity. Similar trends have been reported by Ku et al. [51] using premixed NH_3–CH_4 combustion in a tangential swirl burner. Stable operation was achieved with ~61% NH_3 and 39% CH_4 blends. Nonthermal plasma is attractive for ammonia combustion because baseline NH_3 and CH_4 flames are slow, prone to instability. Nonthermal plasma continuously supplies reactive radicals (OH*, O*, H*) and in rich mixtures generates H_2 in situ, accelerating oxidation and assisting ignition and flame holding. Scientific novelty lies in coupling nonthermal plasma with mechanical swirlers, quantifying radical-pathway control and emissions and validating models/diagnostics for NH_3-blended flames [52].

In addition, measured flame temperature was 1307 °C without plasma assistance and 1316 °C with nonthermal plasma assistance for 100% methane combustion that did not show significant increment and 1442 °C for 80% methane and 20% hydrogen mixture. The difference between the calculated adiabatic flame temperature and the measured temperature can be attributed to the lack of heat insulation in the combustion chamber, which resulted.

5. Conclusions

In conclusion, this study demonstrated that nonthermal plasma-assisted combustion of hydrogen-enriched ammonia and methane blends could enhance flame stability and heat-transfer efficiency, supporting the transition from natural gas to low-carbon renewable gases in existing or newly build industrial applications.

The experiments of hydrogen-enriched ammonia and methane blends demonstrated enhanced infrared emission under nonthermal plasma assistance increases from two principal mechanisms: the modest increases in gas temperature, which amplify continuum (Planck) radiation, and larger populations of reactive and electronically or vibrationally excited intermediates species (e.g., OH*, NH*, NH_2*), which both accelerate chain-branching kinetics and amplify band-emission.

Without nonthermal plasma assistance, pure CH_4 burned with a bright blue cone shame, while CH_4–NH_3 blends form longer yellow flames. The CH_4–H_2 mixtures appeared bright red, in all cases due to hydrogen combustion. The addition of H_2 elevated flame temperature and laminar burning velocity that was observed on ICCD images. With nonthermal plasma assistance, flames became more stable and more intense, exhibiting reduced overall length and visually attached to the base of burner, except the 20% H_2 and 80% CH_4 blend. The lift off the hydrogen–methane could be explained with nonthermal plasma behavior producing high concentrations of transient radicals and vibrationally excited species that accelerated the initiation chain-branching reactions, thereby reducing the local ignition delay.

The nonthermal plasma also increased infrared signal intensities across all H_2-enriched NH_3 and CH_4 blends. For the 80% CH_4 and 20% H_2 case, the H_2O and CO_2 band intensities increased substantially. The 70% NH_3 and 20% H_2 mixture—initially exhibiting comparatively low IR intensity—showed a clear increase under plasma assistance. The strongest measured IR emission intensities for H_2O alone and combined H_2O + CO_2 bands were highest for the 80% CH_4 and 20%H_2 blend that strongly correlated with the highest heat flux, whereas the lowest heat flux occurred for the 70% NH_3 and 20% H_2 blend accompanied with the lowest IR intensities. With plasma assistance, the heat flux of this low-carbon 70% NH_3 and 20% H_2 blend case increased by ~15%. Temperature rises were modest: for pure CH_4 the peak increased from 1307 °C to 1316 °C (~9 °C), while other blends showed increases of approximately 100 K. Chemiluminescence imaging through an NH_2* band-pass filter indicated a broader, more stable reaction zone under plasma, accompanied by greater spatial emission of OH* and NH_2*.

Overall, nonthermal plasma assistance stabilized the flames and increased IR emission through modest gas temperature rises and elevated populations of excited intermediates species, thereby improving heat-transfer efficiency at constant thermal power in H_2-enriched NH_3 and CH_4 blends. Moreover, applying nonthermal plasma to hydrogen-enriched (including rich) flames could significantly enhance thermal radiation heat transfer by strengthening H_2O and CO_2 band emission and supporting practical retrofits from natural gas to low-carbon fuels. Additionally, further investigations are needed to quantify how nonthermal plasma parameters (e.g., discharge power, frequency, duty cycle) influence flame heat flux and radiative heat transfer.

Author Contributions: Writing—original draft, I.A.; writing—review and editing, I.A. and R.P.; conceptualization, I.A. and R.P.; data curation, J.E. and. N.S.; formal analysis, A.J.; methodology, N.S. and A.J.; resources, R.P. and J.E. All authors have read and agreed to the published version of the manuscript.

Funding: This work has received funding from the European Union's Horizon Europe research and innovation program under grant agreement No. 101122257. Views and opinions expressed are, however, those of the authors only and do not necessarily reflect those of the European Union or the European Climate, Infrastructure and Environmental Executive Agency (CINEA). Neither the European Union nor the granting authority can be held responsible for them.

Data Availability Statement: The raw data supporting the conclusions of this article will be made available by the authors on request.

Conflicts of Interest: The authors declare no conflicts of interest. All authors have read and agreed to the published version of the manuscript.

References

1. Bataille, C.; Åhman, M.; Neuhoff, K.; Nilsson, L.J.; Fischedick, M.; Lechtenböhmer, S.; Solano-Rodriquez, B.; Denis-Ryan, A.; Stiebert, S.; Waisman, H.; et al. A Review of Technology and Policy Deep Decarbonization Pathway Options for Making Energy-Intensive Industry Production Consistent with the Paris Agreement. *J. Clean. Prod.* **2018**, *187*, 960–973. [CrossRef]
2. Wesseling, J.H.; Lechtenböhmer, S.; Åhman, M.; Nilsson, L.J.; Worrell, E.; Coenen, L. The Transition of Energy Intensive Processing Industries towards Deep Decarbonization: Characteristics and Implications for Future Research. *Renew. Sustain. Energy Rev.* **2017**, *79*, 1303–1313. [CrossRef]
3. Sara, B.; Guido, M.; Di Gloria, P.; Otón-Martínez, R.A.; Antonio, F.; De Giorgi, M.G. Experimental Characterization And Emission Analysis of Hydrogen-Enriched Fuel Blends in Gas Turbine Applications. In Proceedings of the ASME Turbo Expo, London, UK, 24–28 June 2024; American Society of Mechanical Engineers (ASME): New York, NY, USA, 2024; Volume 3B-2024.
4. Zhang, M.; An, Z.; Wang, L.; Wei, X.; Jianayihan, B.; Wang, J.; Huang, Z.; Tan, H. The Regulation Effect of Methane and Hydrogen on the Emission Characteristics of Ammonia/Air Combustion in a Model Combustor. *Int. J. Hydrogen Energy* **2021**, *46*, 21013–21025. [CrossRef]
5. Patel, V.; Shah, R. Effect of Hydrogen Enrichment on Combustion Characteristics of Methane Swirling and Non-Swirling Inverse Diffusion Flame. *Int. J. Hydrogen Energy* **2019**, *44*, 28316–28329. [CrossRef]
6. Bonuso, S.; Di Gloria, P.; Marseglia, G.; Martínez, R.A.O.; Mehdi, G.; Shah, Z.A.; Ficarella, A.; De Giorgi, M.G. Investigation into the Effect of H2-Enriched Conditions on the Structure and Stability of Flames in a Low-Swirl Combustor Derived from Aero-Engine Design. *Aerospace* **2024**, *11*, 43. [CrossRef]
7. Chai, W.S.; Bao, Y.; Jin, P.; Tang, G.; Zhou, L. A Review on Ammonia, Ammonia-Hydrogen and Ammonia-Methane Fuels. *Renew. Sustain. Energy Rev.* **2021**, *147*, 111254. [CrossRef]
8. Valera-Medina, A.; Xiao, H.; Owen-Jones, M.; David, W.I.F.; Bowen, P.J. Ammonia for Power. *Prog. Energy Combust. Sci.* **2018**, *69*, 63–102. [CrossRef]
9. Valera-Medina, A.; Amer-Hatem, F.; Azad, A.K.; Dedoussi, I.C.; De Joannon, M.; Fernandes, R.X.; Glarborg, P.; Hashemi, H.; He, X.; Mashruk, S.; et al. Review on Ammonia as a Potential Fuel: From Synthesis to Economics. *Energy Fuels* **2021**, *35*, 6964–7029. [CrossRef]
10. Mong, G.R.; Chiong, M.C.; Chong, C.T.; Ng, J.H.; Mashruk, S.; Tran, M.V.; Lee, K.M.; Samiran, N.A.; Wong, K.Y.; Valera-Medina, A. Fuel-Lean Ammonia/Biogas Combustion Characteristics under the Reacting Swirl Flow Conditions. *Fuel* **2023**, *331*, 125983. [CrossRef]
11. Radwan, A.M.; Paul, M.C. Plasma Assisted NH_3 Combustion and NOx Reduction Technologies: Principles, Challenges and Prospective. *Int. J. Hydrogen Energy* **2024**, *52*, 819–833. [CrossRef]
12. Zheng, S.; He, Y.; Liu, H.; Yang, Y.; Lu, Q. Impacts of Radiation Reabsorption on the Flame Speed and NO Generation of CH_4/NH_3/Air Flames. *Energy Fuels* **2023**, *37*, 5632–5643. [CrossRef]
13. Choudhuri, A.R.; Gollahalli, S.R. Combustion Characteristics of Hydrogen±hydrocarbon Hybrid Fuels. *Int. J. Hydrogen Energy* **2000**, *25*, 451–462. [CrossRef]
14. Kurien, C.; Mittal, M. Utilization of Green Ammonia as a Hydrogen Energy Carrier for Decarbonization in Spark Ignition Engines. *Int. J. Hydrogen Energy* **2023**, *48*, 28803–28823.
15. Silva, L.C.P.; Wilfinger, M.M.; Murari, T.B.; Filho, A.S.N.; Moret, M.A.; Santos, A.A.B. Experimental Evaluation of Thermal Radiation and Soot Concentration Rates for Syngas Flames in Lean Condition and Oxygen Enhanced Combustion. *Energy Rep.* **2021**, *7*, 4139–4145. [CrossRef]
16. Hwang, S.S.; Gore, J.P. Characteristics of Combustion and Radiation Heat Transfer of an Oxygen-Enhanced Flame Burner. *Proc. Inst. Mech. Eng. Part A J. Power Energy* **2002**, *216*, 379–386. [CrossRef]
17. Kobayashi, H.; Hayakawa, A.; Somarathne, K.D.K.A.; Okafor, E.C. Science and Technology of Ammonia Combustion. *Proc. Combust. Inst.* **2019**, *37*, 109–133. [CrossRef]
18. Zembi, J.; Cruccolini, V.; Mariani, F.; Scarcelli, R.; Battistoni, M. Modeling of Thermal and Kinetic Processes in Non-Equilibrium Plasma Ignition Applied to a Lean Combustion Engine. *Appl. Therm. Eng.* **2021**, *197*, 117377. [CrossRef]
19. Starikovskiy, A.; Aleksandrov, N. Plasma-Assisted Ignition and Combustion. *Prog. Energy Combust. Sci.* **2013**, *39*, 61–110. [CrossRef]
20. Ghabi, A.; Darny, T.; Dozias, S.; Escot Bocanegra, P.; Pouvesle, J.M.; Sarh, B.; Robert, E.; Boushaki, T. Effects of Pulsed Gliding Arc Plasma on Non-Premixed CH_4/CO_2—Air Flame Stability. *Therm. Sci. Eng. Prog.* **2023**, *40*, 101764. [CrossRef]
21. Varella, R.A.; Sagás, J.C.; Martins, C.A. Effects of Plasma Assisted Combustion on Pollutant Emissions of a Premixed Flame of Natural Gas and Air. *Fuel* **2016**, *184*, 269–276. [CrossRef]

22. Faingold, G.; Kalitzky, O.; Lefkowitz, J.K. Plasma Reforming for Enhanced Ammonia-Air Ignition: A Numerical Study. *Fuel Commun.* **2022**, *12*, 100070. [CrossRef]
23. Chen, W.; Jin, D.; Cui, W.; Huang, S. Characteristics of Gliding Arc Plasma and Its Application in Swirl Flame Static Instability Control. *Processes* **2020**, *8*, 684. [CrossRef]
24. Sun, J.; Wu, H.; Tang, Y.; Kong, C.; Li, S. Blowout Dynamics and Plasma-Assisted Stabilization of Premixed Swirl Flames under Fuel Pulsations. *Appl. Energy Combust. Sci.* **2023**, *14*, 100122. [CrossRef]
25. Choe, J.; Sun, W.; Ombrello, T.; Carter, C. Plasma Assisted Ammonia Combustion: Simultaneous NOx Reduction and Flame Enhancement. *Combust. Flame* **2021**, *228*, 430–432. [CrossRef]
26. Wang, Z.; Aravind, B.; Mashruk, S.; Valera-Medina, A. Numerical Investigation on the Combustion Characteristics of Premixed NH_3-Air Flames Using Gliding Arc Plasma. *J. Energy Inst.* **2025**, *123*, 102314. [CrossRef]
27. Alkhalifa, A.M.; Lacoste, D.A. Thermal and Chemical Effects of Nanosecond Repetitively Pulsed Glow Discharges Applied to an Ammonia–Hydrogen–Air Flame. *Combust. Flame* **2025**, *282*, 114473. [CrossRef]
28. Ehn, A.; Zhu, J.J.; Petersson, P.; Li, Z.S.; Aldén, M.; Fureby, C.; Hurtig, T.; Zettervall, N.; Larsson, A.; Larfeldt, J. Plasma Assisted Combustion: Effects of O3 on Large Scale Turbulent Combustion Studied with Laser Diagnostics and Large Eddy Simulations. *Proc. Combust. Inst.* **2015**, *35*, 3487–3495. [CrossRef]
29. Starik, A.M.; Bezgin, L.V.; Kopchenov, V.I.; Loukhovitski, B.I.; Sharipov, A.S.; Titova, N.S. Numerical Study of the Enhancement of Combustion Performance in a Scramjet Combustor Due to Injection of Electric-Discharge-Activated Oxygen Molecules. *Plasma Sources Sci. Technol.* **2013**, *22*, 065007. [CrossRef]
30. Ombrello, T.; Won, S.H.; Ju, Y.; Williams, S. Flame Propagation Enhancement by Plasma Excitation of Oxygen. Part I: Effects of O_3. *Combust Flame* **2010**, *175*, 1906–1915. [CrossRef]
31. Qi, D.; Ying, Y.; Mei, D.; Tu, X.; Liu, D. Soot Characteristics from Diffusion Flames Coupled with Plasma. *Fuel* **2023**, *332*, 126126. [CrossRef]
32. Shah, Z.A.; Mehdi, G.; Congedo, P.M.; Mazzeo, D.; De Giorgi, M.G. A Review of Recent Studies and Emerging Trends in Plasma-Assisted Combustion of Ammonia as an Effective Hydrogen Carrier. *Int. J. Hydrogen Energy* **2024**, *51*, 354–374. [CrossRef]
33. Fridman, A.; Gutsol, A.; Gangoli, S.; Ju, Y.; Ombrello, T. Characteristics of Gliding Arc and Its Application in Combustion Enhancement. *J. Propuls. Power* **2008**, *24*, 1216–1228. [CrossRef]
34. Paulauskas, R.; Jančauskas, A.; Bykov, E.; Vorotinskienė, L.; Zakarauskas, K. Experimental Study on Luminescence and Thermal Radiation Characteristics of Plasma Assisted-Biogas Flames Changing CO_2 Dilution Level. *Fuel* **2024**, *371*, 132014. [CrossRef]
35. Cozzi, F.; Coghe, A. Behavior of Hydrogen-Enriched Non-Premixed Swirled Natural Gas Flames. *Int. J. Hydrogen Energy* **2006**, *31*, 669–677. [CrossRef]
36. Kalra, C.S.; Gutsol, A.F.; Fridman, A.A. Gliding Arc Discharges as a Source of Intermediate Plasma for Methane Partial Oxidation. *IEEE Trans. Plasma Sci.* **2005**, *33*, 32–41. [CrossRef]
37. Bykov, E.; Striūgas, N.; Paulauskas, R. Emission Spectroscopy of CH_4/CO_2 Mixtures Processed in a Non-Thermal Plasma Augmented Burner. *Catalysts* **2022**, *12*, 1540. [CrossRef]
38. Jančauskas, A.; Paulauskas, R.; Bykov, E.; Zakarauskas, K.; Ambrazevičius, I. Gliding arc plasma effect on thermal characteristics of ammonia/biogas flames. *Therm. Sci. Eng. Prog.* **2025**, *60*, 103494. [CrossRef]
39. Dobó, Z. Heat Radiation Measurement Method for High Pressure Oxy-Fuel Combustion. *Measurement* **2018**, *124*, 191–196. [CrossRef]
40. Miguel, R.B.; Machado, I.M.; Pereira, F.M.; Pagot, P.R.; França, F.H.R. Application of Inverse Analysis to Correlate the Parameters of the Weighted-Multi-Point-Source Model to Compute Radiation from Flames. *Int. J. Heat Mass Transf.* **2016**, *102*, 816–825. [CrossRef]
41. Li, L.; Huang, Q.; Wang, P. An Application of Velocity-Temperature Correction Method with Double Thermocouples in Measuring Standard Flames. *Appl. Therm. Eng.* **2025**, *260*, 125030. [CrossRef]
42. Elias, J.; Faccinetto, A.; Batut, S.; Carrivain, O.; Sirignano, M.; D'Anna, A.; Mercier, X. Thermocouple-Based Thermometry for Laminar Sooting Flames: Implementation of a Fast and Simple Methodology. *Int. J. Therm. Sci.* **2023**, *184*, 107973. [CrossRef]
43. Cafiero, M.; Dias, V.; Iavarone, S.; Coussement, A.; Jeanmart, H.; Parente, A. Investigation of Temperature Correction Methods for Fine Wire Thermocouple Losses in Low-Pressure Flat Premixed Laminar Flames. *Combust. Flame* **2022**, *244*, 112248. [CrossRef]
44. *EN 12953-11:2003*; Shell Boilers—Part 11: Acceptance Tests. European Committee for Standardization (CEN): Brussels, Belgium, 2003.
45. Dagaut, P.; Nicolle, A. Experimental and Detailed Kinetic Modeling Study of Hydrogen-Enriched Natural Gas Blend Oxidation over Extended Temperature and Equivalence Ratio Ranges. *Proc. Combust. Inst.* **2005**, *30*, 2631–2638. [CrossRef]
46. Hayakawa, A.; Arakawa, Y.; Mimoto, R.; Somarathne, K.D.K.A.; Kudo, T.; Kobayashi, H. Experimental Investigation of Stabilization and Emission Characteristics of Ammonia/Air Premixed Flames in a Swirl Combustor. *Int. J. Hydrogen Energy* **2017**, *42*, 14010–14018. [CrossRef]

47. Ayranci, I.; Vaillon, R.; Selçuk, N. Near-Infrared Emission Spectrometry Measurements for Nonintrusive Soot Diagnostics in Flames. *J. Quant. Spectrosc. Radiat. Transf.* **2008**, *109*, 349–361. [CrossRef]
48. Nakaya, S.; Funahashi, T.; Asakami, Y.; Fujio, I.; Takahashi, S.; Tsue, M. Thermometry of Combustion Gas Measuring Two-Band near-Infrared Emissions Less than 1.1 Mm from Water Molecules. *Exp. Therm. Fluid Sci.* **2018**, *94*, 1–8. [CrossRef]
49. Henrion, L.; Sick, V.; Haworth, D.C. A Detailed Experimental and Modeling Comparison of Molecular Radiative Heat Loss in a Spark-Ignition Engine. *Combust. Flame* **2022**, *241*, 112083. [CrossRef]
50. Rocha, N.; Quintino, F.M.; Fernandes, E.C. H2 Enrichment Impact on the Chemiluminescence of Biogas/Air Premixed Flames. *Int. J. Hydrogen Energy* **2020**, *45*, 3233–3250. [CrossRef]
51. Valera-Medina, A.; Marsh, R.; Runyon, J.; Pugh, D.; Beasley, P.; Hughes, T.; Bowen, P. Ammonia–Methane Combustion in Tangential Swirl Burners for Gas Turbine Power Generation. *Appl. Energy* **2017**, *185*, 1362–1371. [CrossRef]
52. De La Torre, M.; Arifur Chowdhury, A.S.M.; Love, N.; Choudhuri, A. Radiative Heat Release from Premixed Oxy-Syngas and Oxy-Methane Flames. *Fuel* **2016**, *166*, 567–573. [CrossRef]